

**Key Points:**

- Dropout signatures in energetic particle fluxes near Dione are basically consistent with a fully absorbing obstacle
- Absorption signatures are found to be asymmetric with respect to the orientation of the moon, pointing to radial drift of electrons
- The deepest absorption signatures were observed at the edge of the low-energy wake pointing to gradient-B drifts

**Correspondence to:**

N. Krupp,  
krupp@mps.mpg.de

**Citation:**

Krupp, N., Kotova, A., Roussos, E., Simon, S., Liuzzo, L., Paranicas, C. P., et al. (2020). Magnetospheric interactions of Saturn's moon Dione (2005–2015). *Journal of Geophysical Research: Space Physics*, 125, e2019JA027688. <https://doi.org/10.1029/2019JA027688>

Received 4 DEC 2019

Accepted 17 APR 2020

Accepted article online 23 MAY 2020

## Magnetospheric Interactions of Saturn's Moon Dione (2005–2015)

**N. Krupp<sup>1</sup> , A. Kotova<sup>2</sup> , E. Roussos<sup>1</sup> , S. Simon<sup>3</sup> , L. Liuzzo<sup>4</sup> , C. Paranicas<sup>5</sup> , K. Khurana<sup>6</sup> , and G. H. Jones<sup>7</sup> **

<sup>1</sup>Max-Planck-Institut für Sonnensystemforschung, Göttingen, Germany, <sup>2</sup>Institut de Recherche en Astrophysique et Planetologie, CNRS, CNES, UPS, Toulouse, France, <sup>3</sup>School of Earth and Atmospheric Sciences, Georgia Institute of Technology, Atlanta, GA, USA, <sup>4</sup>Space Sciences Laboratory, University of California, Berkeley, CA, USA, <sup>5</sup>The Johns Hopkins University Applied Physics Laboratory, Laurel, MD, USA, <sup>6</sup>Institute of Geophysics and Planetary Physics, University of California Los Angeles, Los Angeles, CA, USA, <sup>7</sup>Mullard Space Science Laboratory, University College London, Dorking, UK

**Abstract** The moon Dione orbits Saturn at 6.2 Saturn radii  $R_S$  deep in the Kronian magnetosphere. In situ studies of the moon-magnetosphere interaction processes near Dione were possible with the Cassini/Huygens mission which flew by close to Dione five times at distances between 99 and 516 km. In addition, Cassini crossed Dione's L-shell more than 400 times between 2004 and 2017 and documented the variability of Saturn's magnetosphere. Different flyby geometries allowed to study the interaction processes upstream, in the low-energy wake, and above the north pole of Dione. We describe here the energetic particle measurements from the Low Energy Magnetospheric Measurement System (LEMMS), part of the Magnetosphere Imaging Instrument (MIMI) onboard Cassini. We also use hybrid simulation results from "A.I.K.E.F." to interpret the signatures in the particle fluxes. This paper is a continuation of Krupp et al. (2013, <https://doi.org/10.1016/j.icarus.2013.06.007>) and Kotova et al. (2015, <https://doi.org/10.1016/j.icarus.2015.06.031>). The key results are as follows: (1) Saturn's magnetosphere at Dione's orbit is highly variable with changes in energetic charged particle fluxes by 1–2 orders of magnitude. (2) The dropout signatures near Dione are basically consistent with a fully absorbing obstacle, but some features point to more complex interaction processes than plasma and energetic particle absorption. (3) Absorption signatures are found to be asymmetric with respect to the orientation of the moon, indicative of the presence of radial drift components for electrons. (4) The deepest absorption signatures were observed at the edge of the low-energy wake pointing to gradient-B drifts strongest in that part of the interaction region.

### 1. Introduction

The Cassini mission explored the Saturnian system between 2004 and 2017. The spacecraft orbited Saturn and investigated the Saturnian magnetosphere in the equatorial plane as well as at high latitudes. One of the science goals of the Cassini mission was to explore some of the icy moons in the Kronian system and to investigate their interaction with the local magnetospheric environment. One important aspect is the interaction between the charged particles in Saturn's magnetosphere and the moon nicely summarized by Simon et al. (2015) and more general in Kivelson (2004). During their basic motion with respect to the magnetic field direction (gyrating around, drifting perpendicular to, and bouncing along the planetary field lines), the charged particle interacts with the moon, eventually hitting the moon and is lost. This loss mechanism is measured as absorption signature in the energetic particle fluxes. A detailed interpretation of the depletion profile requires a detailed local electric and magnetic field model in the vicinity of the moon as that controls the access of energetic particles to the surface and/or into interaction regions, such as the wake. This input can be provided by hybrid simulations with a parameter set specifically along the flyby trajectory and based on upstream in situ measurements near the moon. Applying a particle tracing code in such a model helps substantially to interpret the data. The trajectory of the Cassini spacecraft around the ringed planet allowed 38 close flybys at nine different icy satellites and hundreds of crossings of the moon's L-shells. In this paper, we concentrate on five of the close flybys near the icy moon Dione.

Dione has a radius of  $R_{Di} = 561.5$  km and is the fourth largest moon of Saturn. It is embedded deep in the magnetosphere of Saturn and orbits the planet at a distance of 6.28 Saturnian radii  $R_S$  ( $1R_S = 60,268$  km).

©2020. The Authors.

This is an open access article under the terms of the Creative Commons Attribution-NonCommercial-NoDerivs License, which permits use and distribution in any medium, provided the original work is properly cited, the use is non-commercial and no modifications or adaptations are made.

**Table 1**  
*Magnetospheric Parameters at Dione's Orbit*

Parameter	Values	Additional comments	References
Magnetic field, B	75 nT		Simon et al. (2011)
Proton density, $n_p$	2.38–4.39 cm <sup>-3</sup>	Cassini CAPS data	Wilson et al. (2017)
Water group density, $n_{W+}$	14.13–27.84 cm <sup>-3</sup>	Cassini CAPS data	Wilson et al. (2017)
Relative velocity, u	40 km/s		Simon et al. (2011)
Ion composition	Protons and water group ions		
Plasma beta, $\beta$	0.1–0.2	Cassini CAPS data	Wilson et al. (2017)
Proton gyroradius, $r_{g,p}$	500 km		Simon et al. (2015)
Alfvénic Mach number $M_A$	0.37		Simon et al. (2011)

No activity such as plumes or other active sources on the moon have been found on Dione (Buratti et al., 2011) up to date. Therefore, the interaction mainly occurs between the impinging magnetospheric particles onto the surface of the moon and depend on the number, the energy, and mass of the impacting species and the surface material. Since Saturn's magnetosphere is very dynamic at Dione's L-shell with intensity variations of energetic particles of up to an order of magnitude, the number of released or implanted particles on the surface is highly variable as indicated in the range of values listed in Table 1 for reference. So far, magnetic field data alone were inconclusive on whether Dione can also behave as a mass loading obstacle to the magnetospheric flows in Saturn's magnetosphere. Evidence of the presence of  $O^{++}$  at Dione's orbit was concluded by Smith and Tsurutani (1983) from ion cyclotron waves in magnetic field data of the Pioneer 11 spacecraft. Paonessa and Cheng (1985) already pointed out that significant ion losses due to wave-particle interactions should be considered based on the finding of intense ion cyclotron waves found. Magnetic signatures from a tenuous atmosphere around Dione have been studied by Simon et al. (2011), and Saur and Strobel (2005) suggested that Dione may be embedded in a gas envelope based on Voyager data. The plasma instrument CAPS and the mass spectrometer INMS onboard Cassini confirmed that Dione has an seasonally variable exosphere of CO<sub>2</sub> and O<sub>2</sub> (Teolis et al., 2010; Teolis & Waite, 2016; Tokar et al., 2012). Burch et al. (2007) concluded from butterfly pitch angle distributions of low energy ions of that Dione could even supply a distinct plasma torus along its orbit. Tsintikidis et al. (1995) analyzed Voyager 1 plasma wave data and found that in the vicinity of Dione, dust particles are present centered at 2,460 km south of the equatorial plane. The authors interpreted the data as E-ring material or a ringlet associated with Dione. This dust in the vicinity of Dione can also cause absorption signatures in the energetic particle data. Energetic particle results from the Magnetosphere Imaging Instrument (MIMI) in the vicinity of Dione during flybys D1 to D3 have been analyzed by Krupp et al. (2013), and particle tracing results during D1 have been published by Kotova et al. (2015). We revisit the energetic particle measurements onboard Cassini during all the five close Dione flybys and during some of the L-shell crossings far away from the moon Dione itself while also showing the spectra of Dione's upstream environment. In addition the output of the A.I.K.E.F hybrid code for Dione, Flyby D4 was used to trace back charged particles for a better understanding of absorption signatures in the data.

## 2. Instrumentation and Data Analysis

We report here about the results of the energetic electrons and ion measurements during the five Dione flybys of Cassini based on measurements of the Low Energy Magnetospheric Measurement System (LEMMS), part of the MIMI onboard the spacecraft. A full description of MIMI can be found in Krimigis et al. (2004). MIMI/LEMMS was able to measure electrons (15 keV to 21 MeV) and ions (30 keV to 60 MeV) separately. The sensor consisted of two oppositely directed heads. In the low-energy head, electrons and ions were separated by an internal magnet guiding electrons and ions to separate sets of detectors inside the instrument. In the opposite high-energy head, a stack of four detectors were used to separate both species using coincidence criteria between the detectors. During the Dione flybys, this enabled the measurements of two pitch angles at a given time. The time resolution was 5.65 s. Besides the rate channels for electrons (C0 to C7, BE, E0 to E7, and G1) and ions (A0 to A8, B0 to B3, and P1 to P9), MIMI/LEMMS also performed pulse-height analysis for electrons and ions in the so-called PHA E, PHA F1, and PHA A channels where 192 energy

channels were implemented providing a detailed energy spectra. For each data point, we have a magnetic field vector from the MAG instrument described in Dougherty et al. (2004).

### 3. Usage of A.I.K.E.F. Hybrid Code and Particle Tracing Method

The adaptive hybrid model for space plasma simulations A.I.K.E.F. (Müller et al., 2011) is a self-consistent model to describe the local moon-magnetosphere interaction in which electrons are treated as a fluid and ions as individual particles and in which the local disturbances in magnetic and electric fields are taken into account. Kotova et al. (2015) used the simulation output of A.I.K.E.F. for the D1 flyby and compared it with the energetic ion measurements from MIMI/LEMMS. From the comparison of the charged particle tracing results of energetic ions and the measured ions during the upstream Flyby D1, it was concluded that the best fit to MIMI/LEMMS data can only be achieved by introducing significant heavy ion contribution in the MIMI/LEMMS channels. It could also be shown that even small perturbations in the local electromagnetic field parameters as well as the exact plasma parameters and magnetic field magnitude influence substantially the interaction between those magnetospheric ions and the surface of the moon. It is important to note that energetic ions can currently not be included in A.I.K.E.F. in a self-consistent way. Due to the Courant condition, this would require lowering the time step below feasibility (Liuzzo et al., 2019a, 2019b). However, since the densities of the energetic particles are much lower than the low-energy population near Dione, they can be treated simply as test particles.

On the basis of the available A.I.K.E.F. hybrid code simulation of the electromagnetic environment near Dione, we performed the modeling of the MIMI/LEMMS measurements during the close Flyby D4. We use the particle tracing approach and calculated the trajectories of the particles (electrons and ions), which enter the apertures of MIMI/LEMMS and potentially hit the detector. To trace the high-energy particles, we used the numerical method based on the Boris scheme (Boris, 1970), modified for relativistic energies as described in Kotova (2016), Kotova et al. (2019), and references therein. Based on the position and the pointing of MIMI/LEMMS, we traced the trajectories of particles backwards in time for every second along the orbit of Cassini in order to verify if the particles could freely pass the moon or if they would have been lost on it. Inside the volume angle, which corresponds to the opening angle of the MIMI/LEMMS telescopes ( $15^\circ$  for low-energy end and  $30^\circ$  for high-energy end), we traced up to 614 trajectories for the same energy, having in total up to 726,011 trajectories simulated per energy channel per second.

Since MIMI/LEMMS measures differential flux of particles with energies in a certain range, we convert the results of the particle tracing in the following way: We took the average flux measured by MIMI/LEMMS approximately 10 min before the absorption signature and 10 min after, from the corresponding channel and neighboring channels, and we interpolate the average flux into numerous energy steps, such that the sum of subfluxes for every energy step results in the total flux measured by MIMI/LEMMS for this energy channel. Inside the volume angle for every energy step, we assume isotropic flux. Therefore, if some portion of trajectories ends up hitting the moon, we remove the corresponding fraction from the subflux for this energy step.

If the particles hit the moon, we remove these trajectories from the overall population of the particles. In this way, we can reconstruct the absorption signature in the MIMI/LEMMS measurements. The size of the hybrid code simulation box is about  $18 \times 15 \times 15$  Dione radii. Outside the hybrid code simulation box, we used the Khurana magnetic field model (Khurana et al., 2004) for the determination of the background electric and magnetic fields. This model introduces small systematic errors, which, however, may not be too important as the field far away from Dione is quasi-dipolar and adequately represented by the Khurana model. When the particle's trajectory goes outside the simulation box of the A.I.K.E.F. code, we trace it using the Khurana model in order to verify if after mirroring it will come back to Dione's orbital plane significantly far away from the moon or not. If the particles comes back close enough, it enters the A.I.K.E.F. simulation box again. This aspect is also discussed below in Figure 13.

Depending on the local time of the flyby, the noon-midnight electric field as discussed in Roussos et al. (2013) may add/subtract azimuthal velocity of the electrons (around noon or midnight) or drive radial inward/outward motions (maximizing in magnitude at dawn/dusk). Three of the flybys are around the noon-midnight line (see Figure 3), meaning that radial displacements from a noon-midnight electric field are minimized. What its influence is that by enhancing/reducing the corotation velocity is to slightly change the value of the Keplerian resonant energy, a change too small to be resolved with the energy resolution of

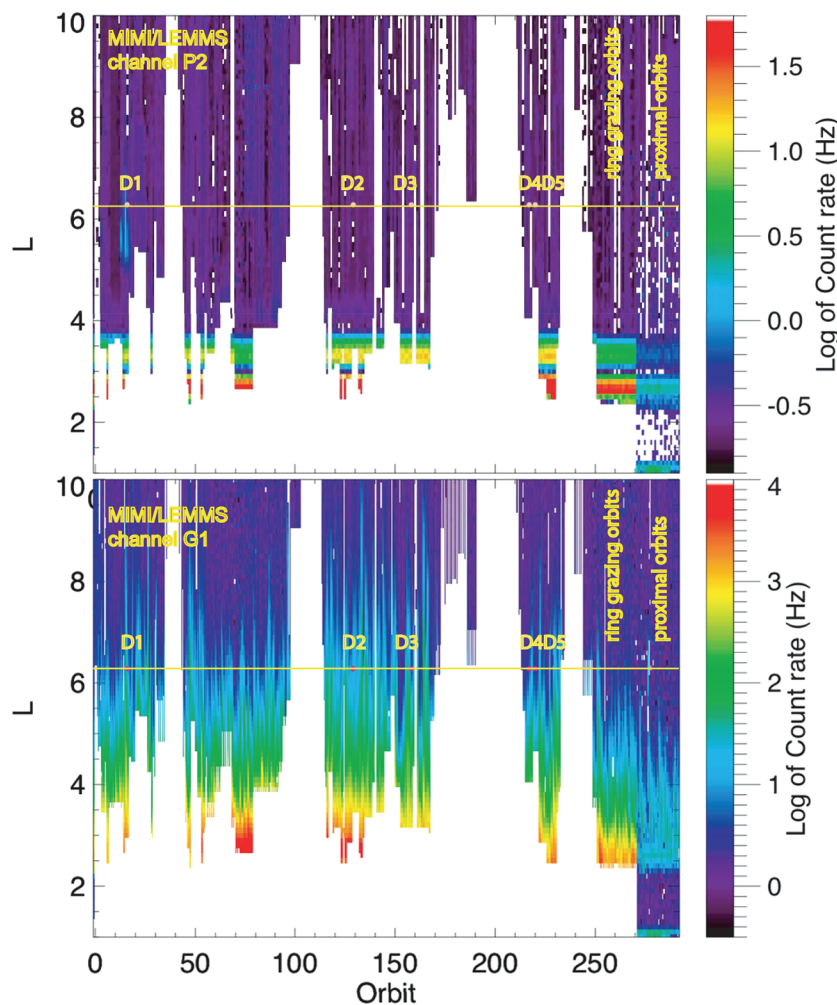


**Figure 1.** Color-coded count rates of protons (Channel P2 [2.3–4.5 MeV]) in the upper panel and electrons (Channel G1 [ $>1$  MeV]) in the lower panel measured with MIMI/LEMMS for the entire Cassini mission as a function of orbit number (time) and L-shell. Dione's L-shell is shown with a yellow horizontal line. The times of the five Dione flybys are marked with D1 to D5.

LEMMS and given also the variability and uncertainty in the strength of corotation. For the rest of the flybys, which are at intermediate local times between the noon/midnight and dawn/dusk lines, some radial inflow/outflow may exist, but its effect is too small to be resolved. Its effect is resolved in microsignatures, that is, aged wakes, because they are exposed to the electric field for hours, a fact that amplifies their offset. Near the moon, depletions are few seconds old, and a few km/sec perturbation by the noon-midnight electric field will only affect them marginally. Also, local magnetic and electric field perturbations are much stronger and easily overwhelm the noon-midnight electric field effects. In any case, it was straightforward to include the electric field in some test-particle simulations, and, as expected, no difference was realized in the output compared to the ones that it was not included.

#### 4. Energetic Particles in Saturn's Magnetosphere at Dione's L-shell

In order to illustrate the dynamics of the Saturnian magnetosphere near Dione, the count rates of MeV particles around Saturn as a function of L-shell were measured by the MIMI/LEMMS sensor 2004–2017 during all 294 orbits around the planet. Figure 1 shows the variability of Saturn's radiation belts for MeV protons (upper panel) and MeV electrons (lower panel) adapted from Roussos et al. (2014), who showed a similar plot for electrons but only for 190 orbits of Cassini. The times of the five close Dione flybys are marked by a dot on top of a yellow line which marks Dione's L-shell. It clearly shows how variable the extent of MeV particle fluxes is in the vicinity of Dione. At keV energies, the magnetosphere is similarly variable. The white gaps

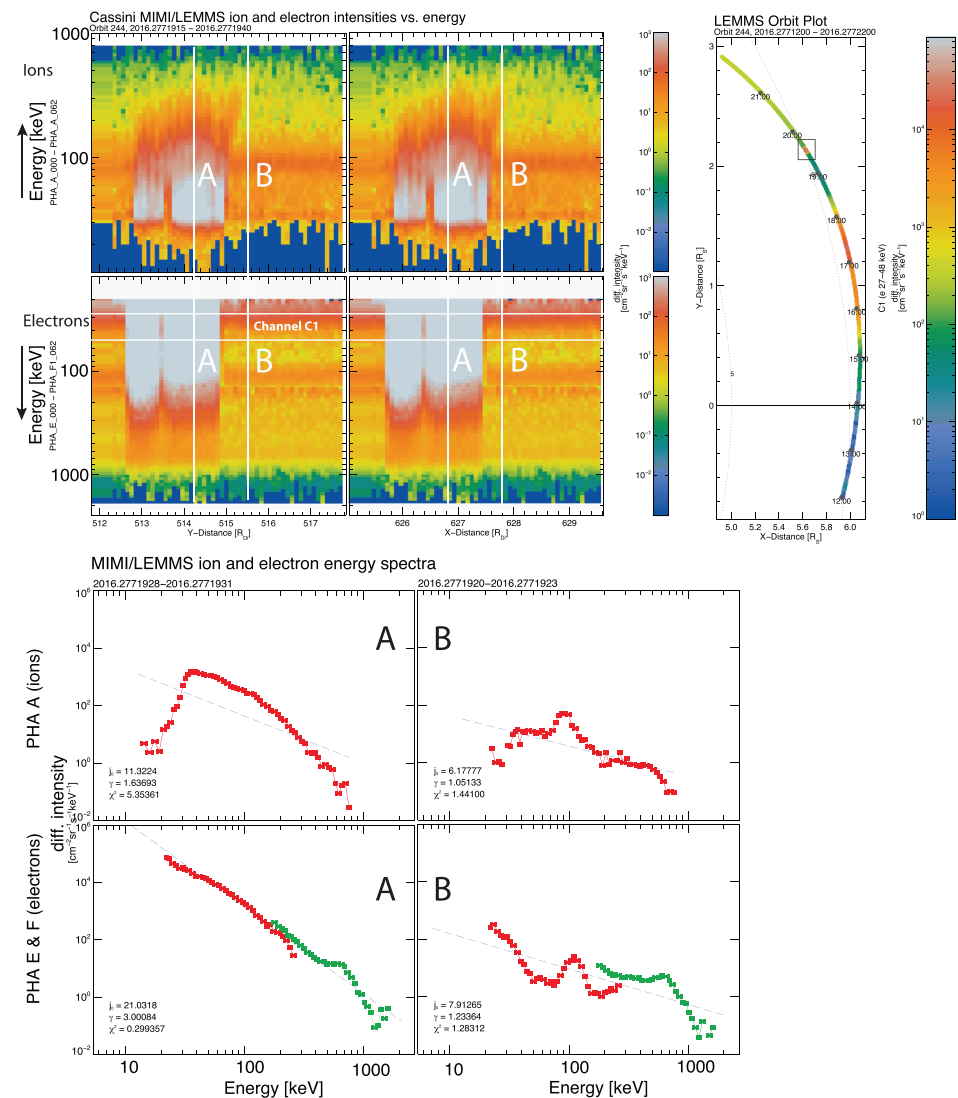


**Figure 2.** Upper left: Color-coded intensities in MIMI/LEMMS pulse height analyzed (PHA) electron channels (lower panel) and PHA ion channels (upper panel) for a Dione L-shell crossing on Day 277, 19:15–19:40 in 2016. On the  $y$  axes, the energy of the PHA channels are plotted (energy increases upward for ions and downward for electrons) as a function of distance  $x$  (positive in the direction of motion of the moon) and  $y$  from Dione (positive  $y$  is the direction toward the planet). The two white lines mark the energy passband of Channel C1 used on the right of the figure. Upper right: Color-coded intensity of electrons in MIMI/LEMMS Channel C1 (27–48 keV) along the Cassini trajectory in Saturn's  $x$ - $y$ -equatorial plane on Day 277, 12:00–22:00 hr in 2016. The dashed circles mark the L-shells  $L = 5$  and  $L = 6$  for reference. The little box marks the time period plotted on the left of the figure. Lower left: Energy spectra of PHA ion channels (upper panels) and electron channels (lower panels) during an ongoing injection event (A) on Day 277 at 19:30 hr or during normal magnetospheric conditions (B) (Day 277 at 19:20 hr).

in this figure mark the orbits where Cassini did not reach the corresponding L-shells. These variable fluxes of charged particles affect the interaction between of the plasma in the magnetosphere of Saturn and the moon Dione. Roussos et al. (2008) found that sometimes even an additional transient radiation belt builds up near Dione's L-shell as a result of externally or internally triggered processes in Saturn's magnetosphere. This can be seen most easily by the enhancement in the P2 fluxes around Flyby D1. On the other hand, sometimes the fluxes near Dione are extremely low, for example, shortly before Flyby D3. Another indication of the dynamics of the Saturnian magnetosphere is shown during the final so-called proximal orbits 2016–2017 of the Cassini mission. Each of those orbits was a week long, and during those time periods, periodic fluctuations were recorded with a period of 2 weeks. These variabilities are discussed in Roussos et al. (2014, 2018, 2019). Sergis et al. (2009, 2011) showed that the thickness of the equatorial plasma sheet which

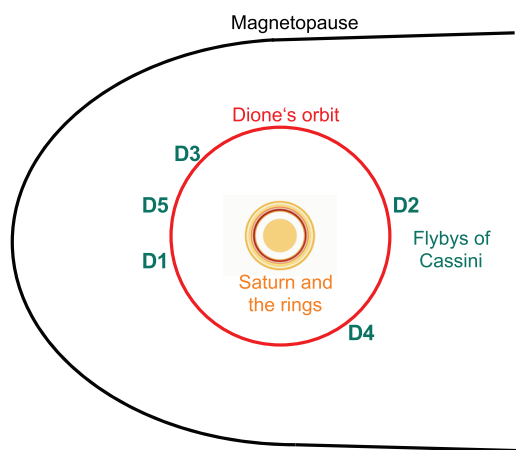


**Figure 3.** Sketch of the five Dione flybys of Cassini in the Saturnian system as viewed from the north onto the equatorial plane (not to scale).

extends between 5 and  $20 R_S$  on the dayside and at least to  $55 R_S$  on the nightside is highly variable between 2 and  $4 R_S$ . The analysis also showed local time and seasonal asymmetries. For details, the reader is referred to the aforementioned papers. All these magnetospheric parameters can influence the interaction between the particles in the magnetosphere in the moon. Cassini crossed the L-shell of Dione in and outbound 418 times. The moon itself was far away from Cassini except during the five close flyby periods described below. The distance to the moon itself varied a lot from orbit to orbit.

Figure 2 shows one example during Dione's L-shell crossing of Cassini on Day 277 in 2016 when an injection of hot plasma was ongoing while Dione was several hundreds of moon radii away. The injection is clearly visible in the energy spectrograms of ions and electrons as sharp intensity increases. The lower four panels of Figure 2 show the detailed ion and electron spectra during the event (A) and before the event (B) at normal magnetospheric conditions. This illustrates how dynamic the magnetosphere of Saturn is in the vicinity of the moons and especially near Dione in this case. A similar injection was ongoing during Flyby D2 with the moon present showing that the responses the MIMI/LEMMS detector onboard Cassini strongly depended on the state of the magnetosphere during the encounter.

The cases of variability discussed above indicate how magnetospheric regions, with the L-shell of Dione included, vary at different time scales, ranging from minutes to months. The amplitude of flux variability is also quite large, as these can change by several orders of magnitude, for both electrons and ions. With that in mind, we may expect that Dione's magnetospheric interaction may transition between different modes. The five Dione flybys by Cassini and the responses of MIMI/LEMMS will be discussed in detail in the following section, as they may hold evidence about these different moon-magnetosphere interaction modes.

#### 4.1. Targeted Dione Flybys D1 to D5 of Cassini

Cassini flew by the moon Dione five times during Flybys D1 to D5. The local time locations of each flyby in Saturn's magnetosphere is shown in the sketch of Figure 3. Flybys D1 and D5 happened close to local noon in the Saturnian system while D2 happened after midnight, D3 in the morning sector, and D4 in the evening sector of Saturn's magnetosphere. Flyby D1 was slightly upstream and south of the moon, D2 and D3 passed the low-energy plasma wake near the equatorial plane, and D4 and D5 were northern polar flybys. The dates and times of the closest approaches (CAs) together with the flyby locations in Saturn local time of all five Dione flybys are shown in Table 2 for reference together with the altitude at CA and the type of flyby geometry.

The trajectories during the five close flybys are illustrated in Figure 4 in two planes of reference relative to Dione in the center of the coordinate system. The upper panels show the trajectories projected onto the equatorial plane, and the lower panels show the projection in a plane perpendicular to it. The differential intensities of electrons in MIMI/LEMMS Channel C1 (27–40 keV) on the left and in Channel E4 (790–4,750 keV) on the right are shown color-coded along the trajectories of the flybys. The low-energy and the high-energy wakes for electrons below and above the resonant energy at the distance of Dione of about

**Table 2**

Dates, Location, Closest Approach Distances, Saturn Local Time, and Type of the Five Dione Flybys D1 to D5 of the Cassini Mission 2005–2015

Flyby	Year	Day and time of CA	Distance at CA (km)	Saturn LT	Type
D1	2005	284 17:52	498	12:39	Upstream south
D2	2010	097 05:16	503	00:49	Wake equatorial
D3	2011	346 09:39	99	09:22	Wake equatorial
D4	2015	167 20:12	516	20:24	Polar north
D5	2015	229 18:33	474	11:18	Polar north

600 keV (assuming 70% of rigid corotation speed) are marked by the shaded yellow areas. The resonant energy is that energy where the electron drift speed and the Keplerian motion of the moon are the same (Thomsen & van Allen, 1980). Electrons with energies above the resonant energy encounter the moon from the opposite direction than the low-energy corotational plasma flow. During the encounter, D1 and D2 particle injections were ongoing during the time of the encounters as already indicated in Krupp et al. (2013). It is obvious during D2 that the dropout feature in Channel C1 (left upper panel of Figure 4) is not aligned with a nominal wake in positive  $x$  direction but slightly shifted toward the planet ( $y$  direction) indicative of a radial flow component, possibly caused by the injection event ongoing. This asymmetry is also consistent with the location of the wakeside compression signature in MAG data (see lower-right panel in Figure 1 of Simon et al., 2011). A similar shift in the dropout feature but in the opposite direction away from the planet is visible in Channel E4 during Flyby D1.

Figure 5 gives an overview of the intensities of ions (upper panels) and electrons (lower panels) as a function of energy and distance from the moon in the direction of Saturn ( $y$  direction) measured in the so-called pulse height analyzed (PHA) channels near Dione during all the five flybys. The PHA channels of MIMI/LEMMS

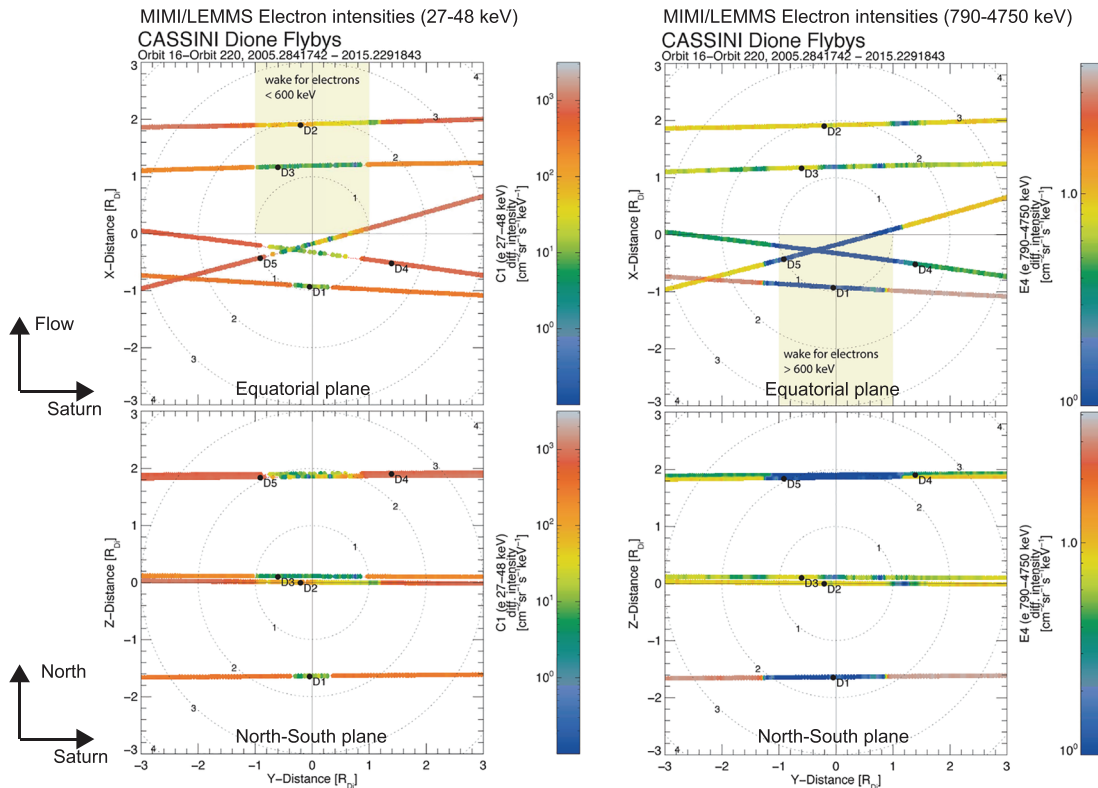


**Figure 4.** Color-coded electron intensities in MIMI/LEMMS Channels C1 (27–48 keV) on the left and E4 (790–4,750 keV) on the right during all five Dione flybys marked with D1 to D5 of the Cassini spacecraft. Dione is in the center of the coordinate system, and the spacecraft trajectories are projected into the equatorial plane (upper panels) and in the north-south plane perpendicular to the equatorial plane (lower panels).

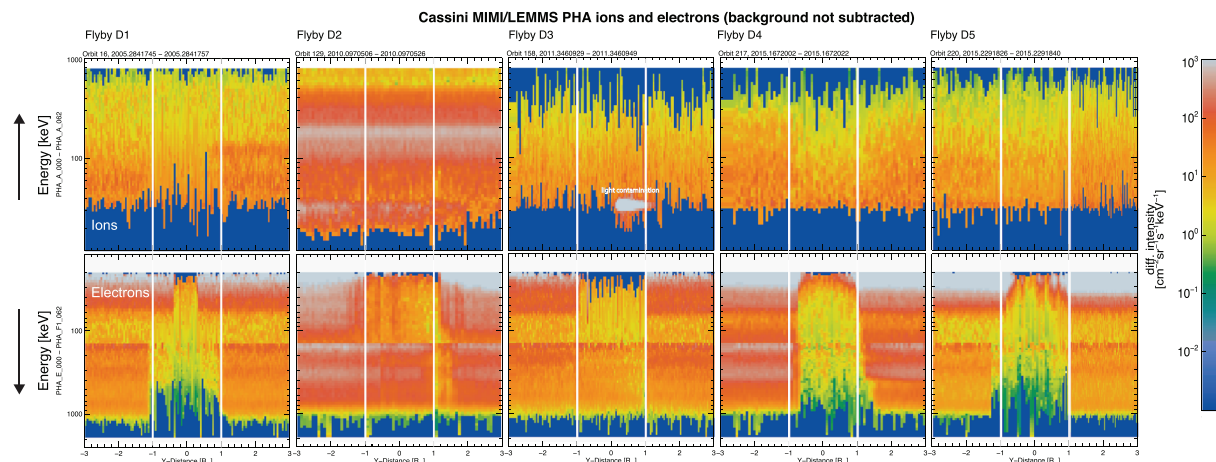


**Figure 5.** Color-coded intensities in MIMI/LEMMS pulse height analyzed (PHA) electron channels (lower panels) and PHA ion channels (upper panels) for all five Dione flybys marked with D1 to D5. On the y axes, the energy of the PHA channels are plotted (please note that the energy increases upward for ions and downward for electrons, so that low-energy particles could be better compared) as a function of distance  $y$  from Dione (positive  $y$  is the direction toward the planet). The white solid lines indicate the width of Dione.

have a very good energy resolution but limited in the energy range shown. In order to better compare the intensities between electrons and ions at low energies, we plotted the energy for ions increasing upward while for electrons downward in the figure. The color intensity scale is the same for all flybys. The electron energy spectrogram is a composite of two separate detectors (E and F) with an overlapping energy range which explains the jump in intensities around 150–200 keV. The white solid lines indicate the width of Dione. The highest intensities in ions were measured during D2 where the values went up by a factor of 5–10 compared to average values. Ion data obtained during the D3 encounter show some light contamination in the lowest energy channels near CA. The responses during the two polar flybys D4 and D5 look similar. Only during D1 and D4 could reduced ion fluxes be observed between the two white lines.

To complete the data set, Figures 6 to 9 represent the particle intensities in a subset of the so-called rate channels (Ion Channels A0 to A4, Electron Channels C0 to C4, and E0, E4, E6, BE) with moderate energy resolution but up to several MeV energies for electrons as a function of  $y$  distance from the moon where  $y$  points toward the planet. These channels cover also the electron energies above the resonant energy drifting in the opposite direction compared to the electrons with energies below the resonant energy. The resonant energy at the orbit of Dione is about 600 keV under the assumption that the plasma is locally corotating with the planet at about 70% of the rigid. The yellow-colored region indicates the width of the moon.

The measurements during Flyby D1 are shown in Figure 6. This flyby has already been partially discussed before in Krupp et al. (2013). The first Dione Flyby D1 was the only one slightly upstream of the moon and south of the equator and therefore the only one where absorption signatures from electrons with energies above the resonant energy were expected. Those electrons are blocked by the entire moon leaving an absorption feature as wide as the moon itself as seen in Channels BE, E4, and E6. It turns out from those measurements that also channels E0 and C4 show a full moon width absorption signature although nominally their energy ranges were below the resonant energy. However, new response simulations have been performed, and it was found that those channels also show responses above the resonant energy of 600 keV (Roussos et al., 2018). This can explain the larger absorption. All the other electron channels only show absorption features much smaller than the moon width and can be explained by the upstream geometry of the flyby. In the lower panel of Figure 6, it is quite obvious that the absorption feature is asymmetric with respect to the yellow-marked region, indicative of a wider absorption than the size of the moon away from Saturn's direction. This implies a local or global radial flow away from the planet. Finally, it is worth noting that the response for Channel E4 shows an asymmetric absorption feature with the deepest absorption at  $y = -1$  at the edge of the yellow-marked area maybe indicative that the drift paths of electrons toward and away from Saturn are not identical. The next two flybys, D2 and D3, crossed through the low-energy wake of the moon at different distances. D2 occurred further away than D3. The energetic particle measurements are summarized in Figures 7 and 8.

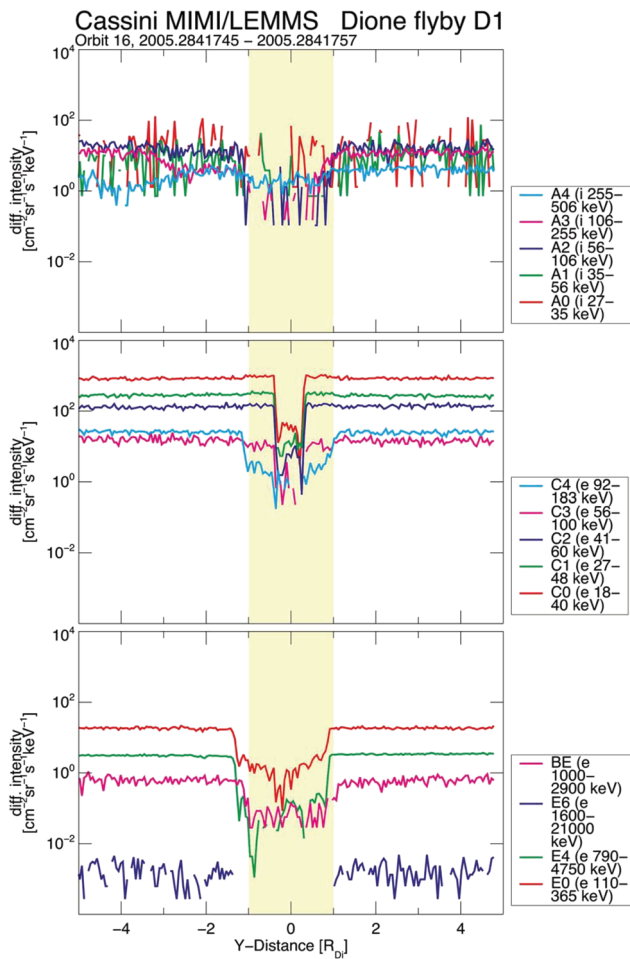


**Figure 6.** Cassini MIMI/LEMMS measurements of ions at various energies in Channels A0 to A4 (upper panel) and of electrons with keV to several MeV energies (middle and lower panels) during the D1 Dione flyby. While the C and BE channels measure electrons from the low-energy end of the sensor, the E-channels register electrons from the opposite side (high-energy end of the sensor). The yellow-marked region indicates the width of the moon.

For both flybys, no absorption signatures in the low-energy ions could be observed. During Flyby D3, Channel A0 was contaminated by sunlight due to a reorientation of the spacecraft. During Flyby D2, the magnetosphere was quite disturbed with fluxes before and after the encounter being different. The absorption signatures of electrons below the resonant energy were slightly wider than the geometric wake and showed an asymmetry with a deeper absorption at the edge of the wake toward Saturn in both cases. Also, in the electron channels above the resonant energy, a bite-out feature near the edge could be observed.

The final two flybys, D4 and D5, happened in 2015 and passed over the north pole of Dione with CAs at 516 and 474 km from the moon, respectively. Both flybys showed a notable, energy-independent wake offset away from the planet ( $y < 0$ ) as visible in Figures 9 and 10. We first discuss Flyby D5 (Figure 9). MIMI/LEMMS ion and electron measurements during Flyby D5 are shown for different channels: A0 to A4 (ions 27–506 keV), C0 to C4 (electrons 18 to 183 keV), and E0, E4, E6, BE (electrons 110–21,000 keV). No significant ion losses are visible, while for all electron channels shown, strong absorption features are visible. The fluxes were highly variable when the spacecraft moved across the polar region (yellow-shaded region in Figure 9) except for Channel E6 where the count rates are very low and close to background. The widths of the absorption signatures of Electron Channels C0 to C2 were as wide as the moon or slightly smaller, while for higher energies in Channels C3, C4, BE, E0, and E4, the absorption widths were wider than the moon itself. Similar features were observed during Flyby D4 in Figure 10. The absorption can clearly be seen in Channels C0 to C4, BE, E0, E4, and in the Ion Channels A0 to A4 but much less pronounced. Electron Channel E6 is again too noisy to see a clear absorption. For Electron Channels C0, C1, and C2, the width of

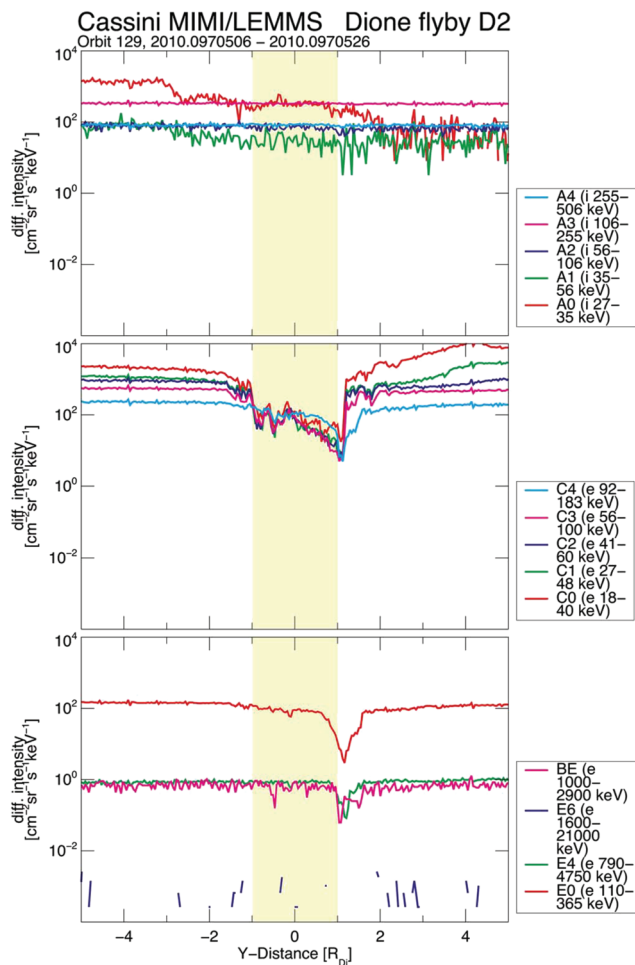


**Figure 7.** Cassini MIMI/LEMMS measurements of ions and electrons during the Dione Flyby D2. Same format as Figure 6.

the absorption is smaller than the size of the moon. For the other electron channels and the ion channels, it is similar to the moon size or even a little bit larger. Comparing the measurements of D4 and D5, it is obvious that the shapes of the dropouts in the electron channels are slightly different and slightly steeper during D4 versus D5. The variability when crossing the polar region marked by the yellow-shaded area is stronger during D5. If these features are distance or time dependent remains unclear.

For Flyby D4, the output from the A.I.K.E.F. hybrid code for magnetic field magnitude and particle density during Dione Flyby D4 is available and shown in Figure 11. The white contour lines represent the magnetic field lines stream lines in the left column and the velocity stream lines in the right column. Using the particle tracing approach and the parameters from A.I.K.E.F. we simulated the MIMI/LEMMS observations during Flyby D4 and reproduced the absorption signatures in the Electron Channels C0 to C4 and BE (measured with the low-energy end) and E0, E4 (measured with the high-energy end) very well as shown in Figure 12.

The level to which the simulation reproduces the data depends on the species, energy, and spatial scales over which we perform the comparison. Deviations of the model output from the data can be associated to issues in data quality and/or to the assumptions in the model and the tracing methodology.

For ions, for instance, we did not obtain any simulated absorption signature in the energy ranges corresponding to the Ion Channels A3 and A4, unlike what is seen in the data. The explanation can be twofold. One scenario is that ion channels are affected by instrument penetrating electrons, meaning that the signal dropout seen is in reality a penetrating electron depletion rather than an ion absorption. An alternative is that energetic ions are depleted after “returning” to Dione’s interaction region through their large gyro-motion, a scenario which is difficult to accurately simulate with our tracing approach. The way that such

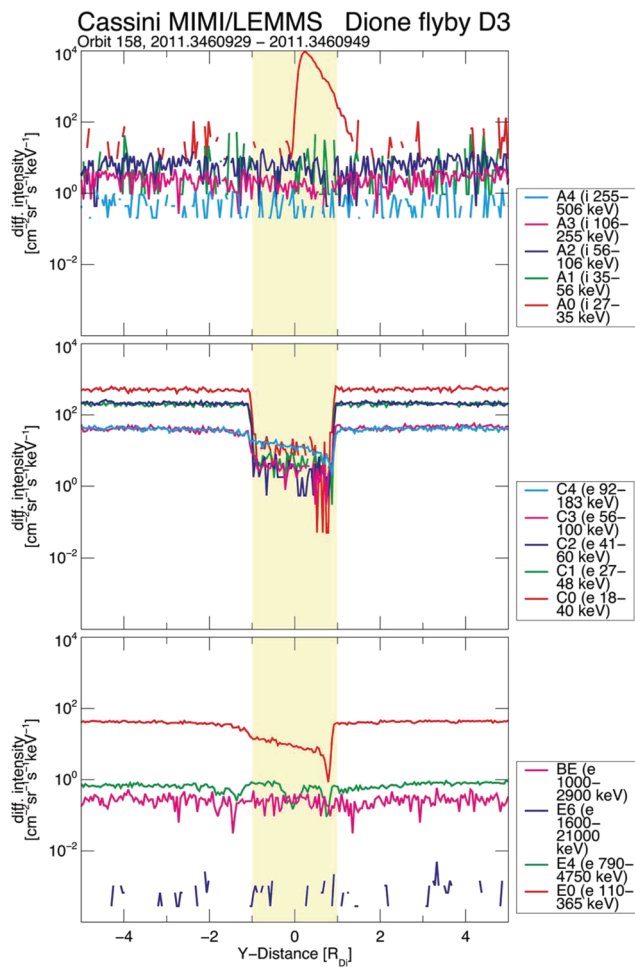


**Figure 8.** Cassini MIMI/LEMMS measurements of ions and electrons during the Dione Flyby D3. Same format as Figure 6. Please note that the differential intensity for Channel A0 in the upper panel is light-contaminated and not real.

“returning” ions are treated in the simulation depends on the estimation of the E and B fields values outside the hybrid code simulation box, as explained below.

During the D4 flyby, the low-energy end of MIMI/LEMMS pointed away from the moon, as illustrated in Figure 13. The right panel shows the projection in the x-y plane (equatorial plane), and the left panel shows the same plot but its projection in the x-z plane perpendicular to the equatorial plane. Here, we depicted the orbits of Cassini and Dione (violet and green lines, respectively), MIMI/LEMMS pointing (short red lines point away from the Cassini orbit), and the trajectories of an electron (18 keV) and an ion (255 keV proton). The red star shows the position of an ion when it enters the MIMI/LEMMS detector, and the blue sphere indicates the position of Dione at this moment. The orange star shows the position of this ion, when it crossed the equatorial zone during the previous bounce period, about 70 s before it enters MIMI/LEMMS. Finally, the gray sphere indicates the position of Dione at that moment. Figure 13 clearly shows that for the specific MIMI/LEMMS pointing and Cassini position, an electron in the vicinity of Dione will bounce near the moon due to local magnetic field gradient. This is exactly what has been seen at Jupiter’s moon Callisto for electrons (see Figure 5 in Liuzzo et al., 2019b). Due to its fast bounce period, its trajectory intersects Dione, and the particle is removed and contributes to the simulated depletion signature of MIMI/LEMMS. Throughout this simulation, the electron’s small gyromotion and low-altitude mirror point keeps it within the boundaries of the simulation box. Contrary to that, a proton with a much larger gyroradius has its mirror point well outside the hybrid code simulation box. Even though the simulated ions have the same pitch angle as the electrons, their large gyroradius make them insensitive to local magnetic field gradients near Dione, such that their mirror point is at higher altitudes from Dione (or magnetic latitudes) and thus outside the

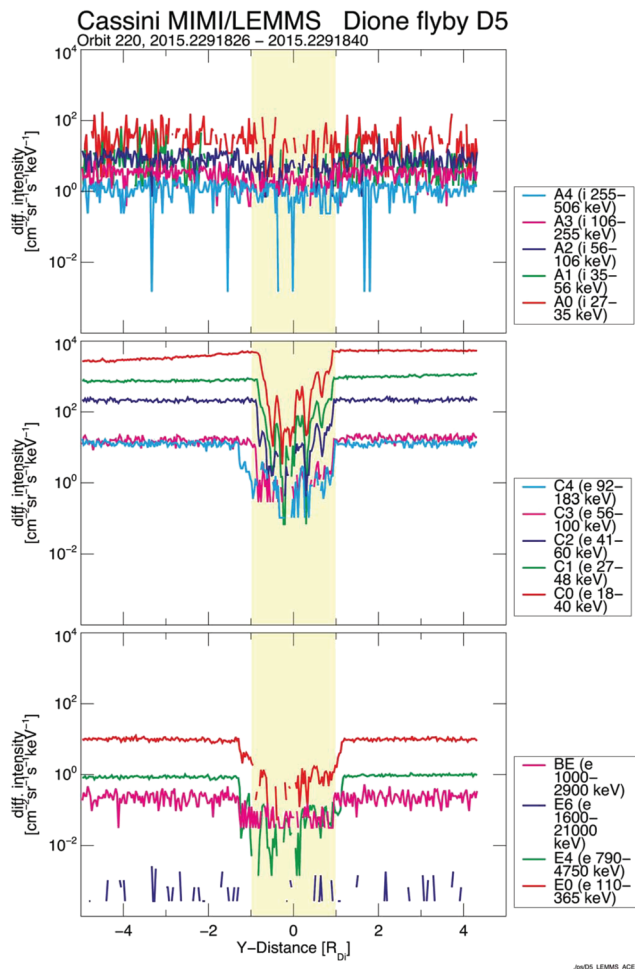


**Figure 9.** Cassini MIMI/LEMMS measurements of ions and electrons during the D5 Dione flyby. Same format as Figure 6.

simulation box. This proton comes back to the equatorial plane far away from Dione, and in the simulation, it won't be absorbed. However, it can be seen in this figure that this ion is passing relatively close to the moon. The majority of the ion's path was outside the hybrid code simulation box where the electromagnetic fields were calculated on the basis of the Khurana magnetic field model, which offers an average description of the magnetospheric field, ignoring moon disturbances. In that respect, the tracing of an ion's trajectory all the way to the mirror point and back may lead to significant error accumulation, such that we cannot exclude that a certain fraction of ions with similar trajectories was actually absorbed not directly before entering to the MIMI/LEMMS detector but half a bounce period before. Since this effect is difficult to quantify, we refrain from interpreting the ion depletion further, although we expect that penetrating radiation is the most likely explanation for the observations. Energetic electrons are more rich in interaction features, and thus model-data comparisons may be more revealing about aspects of the moon-magnetosphere interaction. First, we notice that the locations where LEMMS and the simulations show sharp dropouts, essentially the sharp wake flanks, are in good agreement. Where data and simulations mostly disagree are in the wake depths. Electron flux depletion levels in C3 and C4 are predicted to be much weaker than seen in the data. At higher energies, Channels E0 and E4 show shallower depletions than simulations predict. Furthermore, the absence in the simulations of an extended, gradual flux dropout at the Saturn-facing side of the wake, which in MIMI/LEMMS observations is seen in Channels C3, C4, E0, and E4, is also an apparent model-data disagreement. We discuss all these features below.

First, the good agreement of the predicted and observed sharp wake boundaries indicates that at least for Flyby D4, an upstream, radial magnetospheric flow component is not required to explain the observations, as no such component is included in the simulations. The offset of the electron wake boundary location at

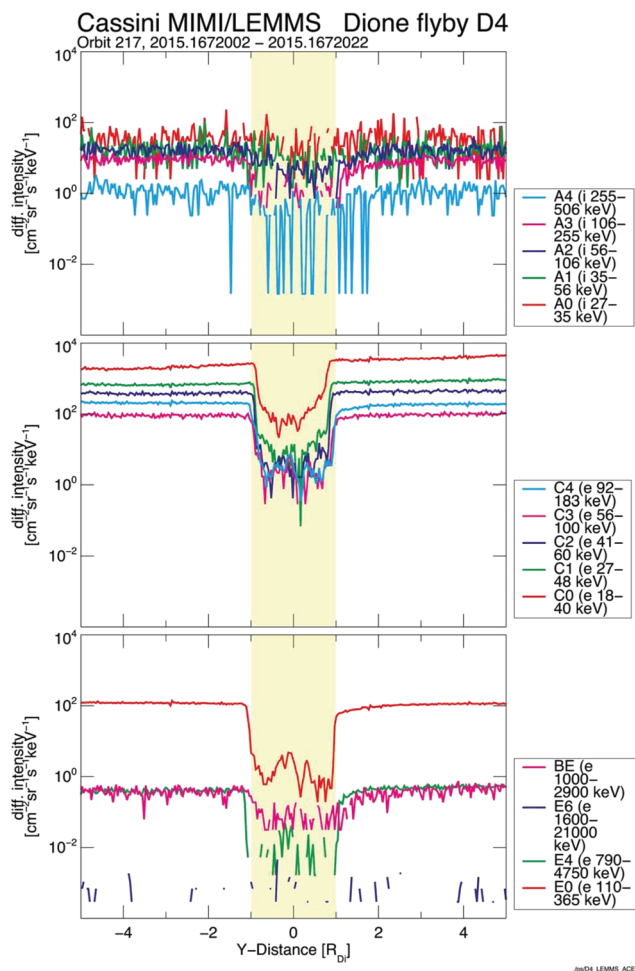


**Figure 10.** Cassini MIMI/LEMMS measurements of ions and electrons during the Dione Flyby D4. Same format as Figure 6.

the anti-Saturn facing side of the wake (Figure 5—D4 electron panel,  $y < 0$ ) is likely a simple geometrical effect: At the wake flanks ( $y \sim 1 R_{Di}$ ) and along the  $x$  direction of the main electron drift motion, Dione's effective obstacle size is very small ( $x_{eff}[R_{Di}] = 2\sqrt{1 - y^2} \sim 0$ ), over which electrons may bounce above or below and evade absorption.

At the Saturn-facing side of the wake flanks ( $y > 0$ ), the dropout wake boundary is energy dependent, and only an approximate, energy-independent location is predicted by the simulations. Krupp et al. (2013) demonstrated, using a guiding-center simulation approach developed for equatorially mirroring electrons, that an energy-dependent broadening of the wake, asymmetric between the  $y > 0$  and  $y < 0$  sides, can develop if a random, diffusive electron motion is also taken into account. Magnetic field gradients across the  $y < 0$  wake flanks favor diffusive electron entry over the gradients at  $y > 0$ , at least for equatorial mirroring particles. In essence, the observed broadening should have been on the reverse wake flank compared to the one seen in MIMI/LEMMS during D4. We note, however, that in D4, MIMI/LEMMS is not measuring equatorially mirroring electrons and that the flyby is upstream with respect to the deep wake of Dione, in a region where the distribution of field gradients is different. A diffusive motion component is not yet included in the present, full motion tracing simulations and could be further explored for particles that mirror away from the equator and experience the local magnetic field disturbances near Dione for less time. This diffusive component refers to the stochastic motion of electron guiding centers due to natural fluctuations in the background electromagnetic field (e.g., ULF waves). We observe its effects in the refilling of the microsignatures (radial diffusion). The radial velocities involved with this stochastic motion are small but can become important for electrons which drift slowly with respect to the moon (i.e., around the Keplerian resonant energy), and they can fill up a wake much close to the moon than much higher or much

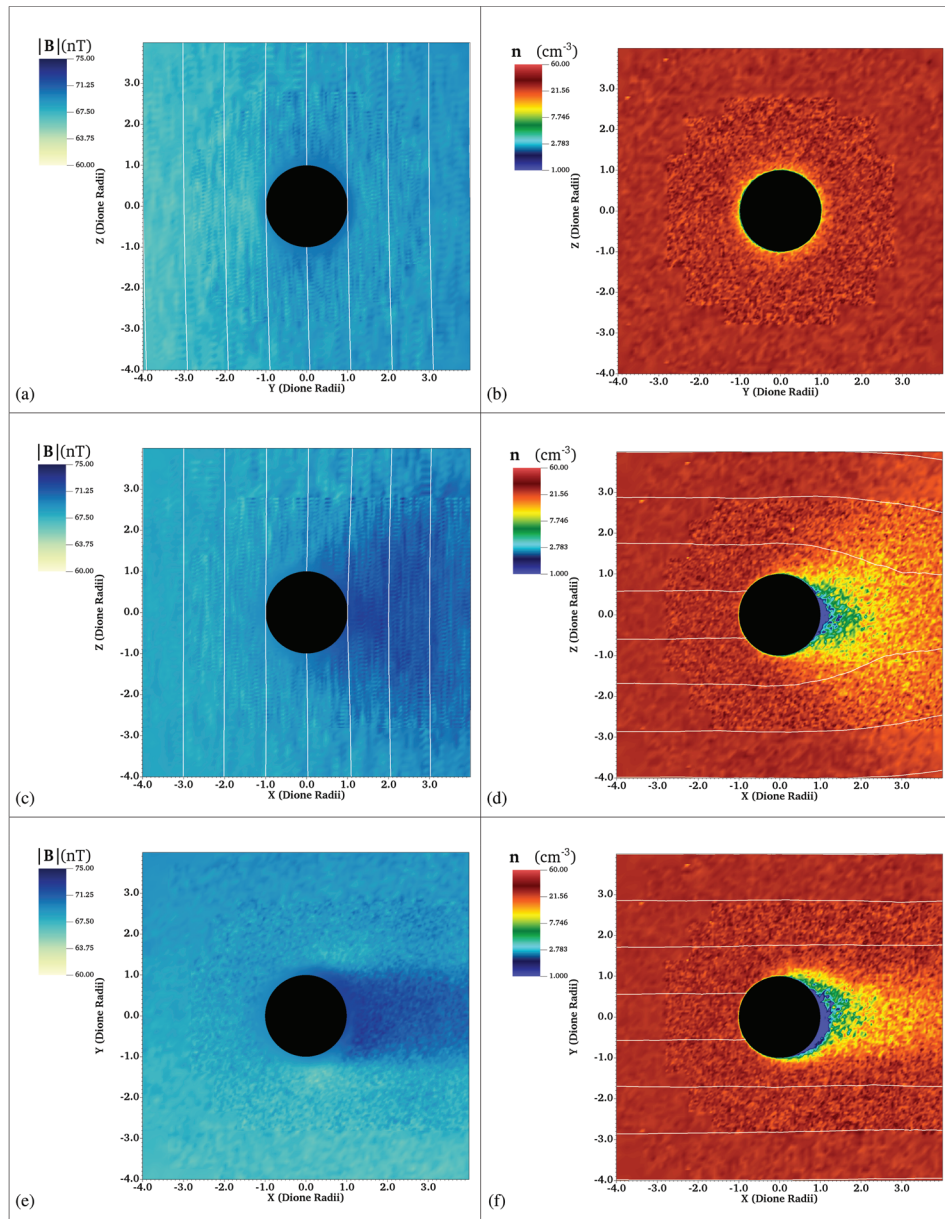


**Figure 11.** A.I.K.E.F. output of magnetic field Magnitude  $B$  (plots a, c, and e) and particle density  $n$  (plots b, d, and f) around Dione during the Flyby D4. The color-coded  $B$ - and  $n$ -values are shown in the  $y$ - $z$  plane (upper row),  $x$ - $z$  plane (middle row), and  $x$ - $y$  plane (bottom row) where Dione is in the center of the coordinate system,  $x$  points in the direction of orbital motion of the moon,  $y$  points toward Saturn, and  $z$  points north. Magnetic field streamlines in the (a)  $y$ - $z$  plane and (c)  $x$ - $z$  plane are displayed, while bulk flow velocity streamlines in the (d)  $x$ - $z$  plane and (f)  $x$ - $y$  plane are included. Streamlines are omitted from plots (b) and (e), which display planes that are nearly perpendicular to the flow velocity and magnetic field, respectively.

lower energy electrons. The inclusion of a diffusive component in the simulations will be explored in future studies, not limited to Dione but to different moons of Saturn and Jupiter.

The disagreement in depletion depth in Channels C3 and C4 is likely due to the impact of penetrating MeV electrons in these channels, similar to the case of the MIMI/LEMMS ion channels. Essentially, C3 and C4 show us how MeV electrons are lost, rather than the keV electrons they were designed to measure. We believe this is the case because the residual signal profile within the observed electron depletion of C3 and C4 is similar to the residual of higher energy channels. Furthermore, C3 and C4 show the same gradual flux

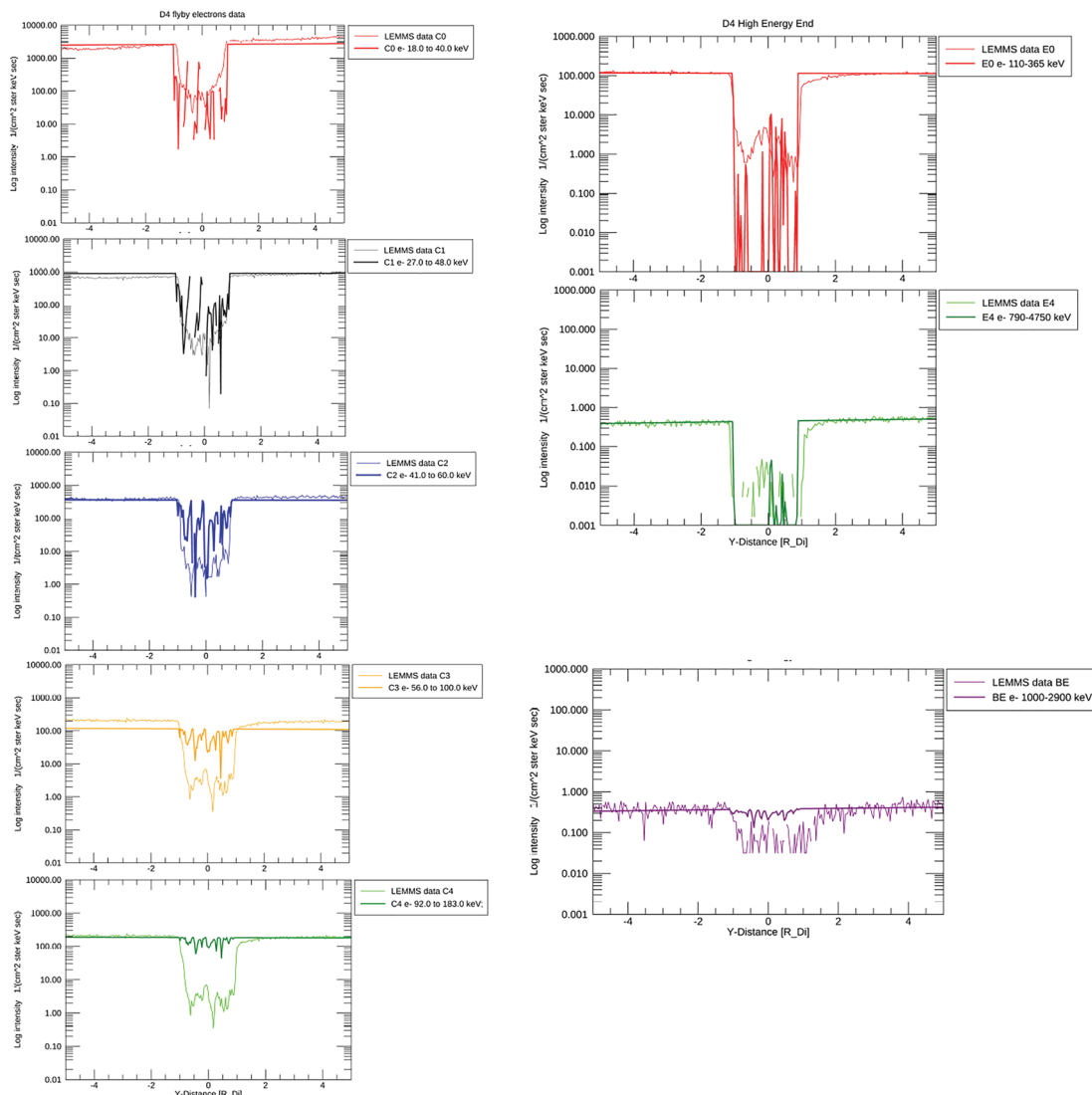


**Figure 12.** MIMI/LEMMS electron measurements during Dione Flyby D4 in comparison with the particle tracing results on the base of the A.I.K.E.F. hybrid code simulation. Left: intensities of Electron Channels C0 to C4 (measured with the low-energy end) in the energy range 18–183 keV; right: intensities of Channels E0 and E4 (measured with the high-energy end) and BE (low energy end) in the energy range 110–2,900 keV plotted in the same coordinate system as in Figures 6–9. The vertical dashed lines indicate the closest approach of Cassini to Dione.

dropout in the Saturn-facing side of the wake, which is prominent in the higher energy channels (E0 to E4) but not in the neighboring Channels C0–C2.

The very deep dropout that is simulated in the higher energy E-channels originates from the fact that these channels belong to MIMI/LEMMS's high energy telescope, which for D4 was pointing toward the surface, that is, measuring electrons coming directly from the region that Dione obscures electron motion very efficiently. It is interesting that MIMI/LEMMS data indicate that even above Dione, some small but detectable residual electron signal is detected. As Dione is unlikely to be a source of electrons at 100 keV to a few MeV, it is likely that at very low altitudes, the magnetic field is enhanced more significantly than predicted by the hybrid simulation (Figures 11a, 11c, and 11e), such that a small fraction of electrons coming from north latitudes mirrors and is reflected back toward MIMI/LEMMS before it gets absorbed by Dione.

## 5. Summary and Conclusions

Cassini MIMI/LEMMS measurements in the vicinity of the moon Dione have been analyzed. It was noticed that the magnetosphere in the vicinity of Dione is highly dynamic with count rate variability of 1–2 orders of

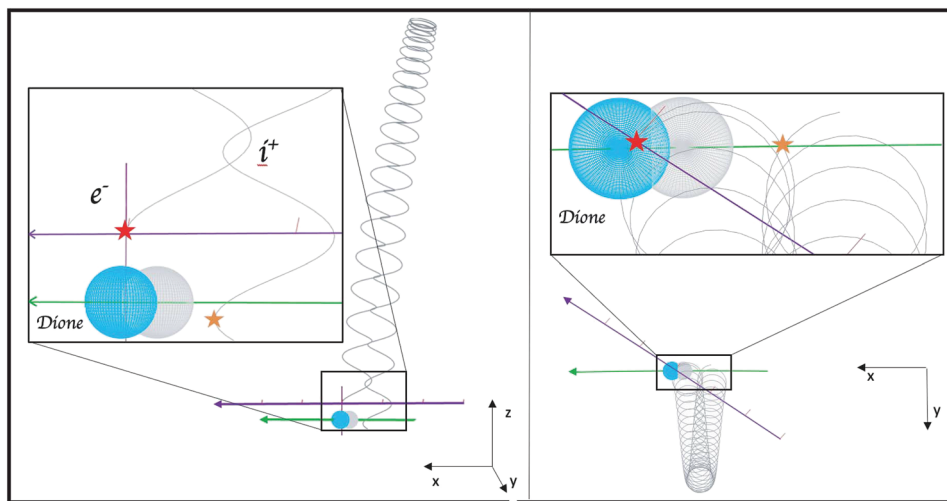


**Figure 13.** Cassini passage over Dione during the D4 flyby. Violet and green lines show the orbits of Cassini and Dione, respectively, and short red lines indicate the LEMMS pointing every 200 s. The purple trajectory is that of an electron (18 keV) moving backwards in time from the LEMMS entrance at the time of closest approach; this trajectory intersects the moon after mirroring. Gray trajectory is a trajectory of a proton (255 keV) which also comes back to the neighborhood of the moon after mirroring but farther away from the moon.

magnitude. During the five close flybys of Cassini at Dione, the MIMI/LEMMS spectrometer measured the locally absorbed charged particles with the limitations of spacecraft orientation and corresponding viewing geometry of MIMI/LEMMS during the flybys. With the modeled magnetic field during Dione Flyby D4 derived from the hybrid code A.I.K.E.F. we were able to reconstruct aspects of the absorption features in the MIMI/LEMMS electron data by comparing them with the results of particle tracing in the locally disturbed magnetic field. A series of features that could not be reproduced by the simulations were also discussed, as they offer useful context for understanding Dione's magnetospheric interaction and its impact on energetic electrons and ions. In certain cases, the disagreements were due to spurious instrument responses, which are also important to identify in order to avoid misleading interpretations.

Among our key results are asymmetries in the absorption signatures from energetic electrons with respect to the orientation of the moon during upstream Flyby D1 where the whole absorption dropout region in the electron intensities was shifted away from Saturn, indicative of a radial electron drift component either in the magnetosphere or in the local moon-magnetosphere interaction environment. Independent of the origin of the radial flow component, its presence was expected to result to an energy-dependent wake boundary location because the azimuthal drift of electrons (corotation + magnetic drifts) strongly depends on energy. For electrons drifting slowly in azimuth, radial drifts become a larger fraction of their total drift velocity, thus a stronger offset would be expected for the wake at their corresponding energy (and the contrary). In that respect, the absence of an energy-dependent wake location at D1 is a mystery. In the case of D4, a similar offset could be explained by simple geometrical considerations, which however do not apply in the case of D1, where the wake is displaced away from the expected location of Dione's flux tube at  $y < 0$ . The same mystery applies for Flyby D5, where an energy-independent wake location is offset away from Dione's position at  $y < 0$ . Another asymmetry was found during D2 and D3 in electron depletions where the deepest depletion occurred near the edge of the low-energy wake on the side toward the planet. The possible reason has already been described in detail in Krupp et al. (2013). Basically, it is the result of the gradient-B having different signs in the Saturn-facing and anti-Saturn-facing sides of the wake flanks. This asymmetry was less obvious in D1, D4 and D5, which, however, occur more upstream with respect to the plasma wake of Dione, where electrons experience different field gradients. This may explain, for instance, also the energy-dependent wake broadening seen in electrons at the Saturn's facing side of the wake during D4.

Overall, in most cases, MIMI/LEMMS data in the vicinity of Dione are consistent with a fully absorbing obstacle, even during Flyby D1, that in earlier studies using magnetometer observations, it shows elements of a mass-loading interaction. However, there are signatures that remain unexplained (e.g., broader depletions in D4 and D5, asymmetries in plasma wake, lack of energy dependence in radial position of wake, and

signature of field-aligned current in the wake flank of D4). This means that the simplest form of interaction assumed in this paper, a plasma and energetic particle absorption, is maybe not good enough to describe the complex interaction processes. It is possible that in the wake, where heavy plasma losses overwhelm the effects of a weak mass loading source, we see predominantly the signatures of an absorber. Upstream of the wake and before Dione has absorbed a significant amount of the upstream magnetospheric plasma, the presence of a weak mass loading source is making its presence more prominent. We may therefore be dealing with a bimodal magnetospheric interaction. Bimodal simply means that the interaction can behave both as a plasma-absorbing and as a plasma-loading one. Because Dione does not have an internal source of neutrals and therefore plasma (as e.g., Io or Enceladus), how much it loads the magnetosphere with plasma depends on how strong or weak its exosphere is. In turn, the exospheric properties may derive partially by enhanced sputtering conditions from the environment which is known to be variable (e.g., see example of strong injection included in the paper). Evidence that Dione may behave as plasma loading body is in the studies of Khurana et al. (2008) and Simon et al. (2011). It may also be that the mass loading signatures observed at Dione and discussed in the two studies are only resolvable upstream, before particle absorption occurs. Downstream, losses of plasma are always too strong to be balanced by mass loading (even if it does occur), which is why magnetic field was always getting enhanced in the wake. If we want to understand the current balance, we should have in mind that mass loading in the wake, even if it is weak, may reduce the level of magnetic field enhancement, which is why it is useful to think Dione's interaction as bimodal. This bimodality may be regulated by how deep in the wake or how far upstream of Dione we are making observations, but also from the state of the highly variable upstream plasma and energetic particle environments, which control the state of Dione's exosphere and the strength of its possible mass loading source.

### Data Availability Statement

The Cassini data used in this study are available online through NASA PDS using the following link: <https://pds-ppi.igpp.ucla.edu/mission/Cassini-Huygens/CO/MIMI>.

### Acknowledgments

The German contribution of the MIM/LEMMS Instrument was in part financed by the DLR (Deutsches Zentrum für Luft- und Raumfahrt e.V.) under Contract Nos. 50 OH 1101 and 50 OH 1502 and by the Max-Planck-Gesellschaft. The JHUAPL portion of this work was supported in part by a NASA contract NAS5-97271 under task 006. The work of Lucas Liuzzo and Sven Simon was supported by NASA through the Cassini Data Analysis and Participating Scientists (CDAPS) 2014 program, Grant NNX15AH12G. Lucas Liuzzo was also supported NASA SSW Grant number NNX15AL20G. The work of Anna Kotova was supported by CNES. We thank Andreas Lagg (MPS) and Jon Vandegriff (JHUAPL) for providing powerful software packages to analyze the MIMI/LEMMS data set.

### References

- Boris, J. P. (1970). Relativistic plasma simulation-optimization of a hybrid code. Proceeding of Fourth Conference on Numerical Simulations of Plasmas.
- Buratti, B. J., Faulk, S. P., Mosher, J., Baines, K. H., Brown, R. H., Clark, R. N., & Nicholson, P. D. (2011). Search for and limits on plume activity on Mimas, Tethys, and Dione with the Cassini Visual Infrared Mapping Spectrometer (VIMS). *Icarus*, 214, 534–540. <https://doi.org/10.1016/j.icarus.2011.04.030>
- Burch, J. L., Goldstein, J., Lewis, W. S., Young, D. T., Coates, A. J., Dougherty, M. K., & André, N. (2007). Tethys and Dione as sources of outward-flowing plasma in Saturn's magnetosphere. *Nature*, 447, 833–835. <https://doi.org/10.1038/nature05906>
- Dougherty, M. K., Kellock, S., Southwood, D. J., Balogh, A., Smith, E. J., Tsurutani, B. T., et al. (2004). The Cassini magnetic field investigation. *Space Science Reviews*, 114, 331–383. <https://doi.org/10.1007/s11214-004-1432-2>
- Khurana, K., Arridge, S. C., & Dougherty, K. M. (2004). A new global model of Saturn's magnetospheric field. AGU Fall Meeting Abstracts.
- Khurana, K. K., Russell, C. T., & Dougherty, M. K. (2008). Magnetic portraits of Tethys and Rhea. *Icarus*, 193, 465–474. <https://doi.org/10.1016/j.icarus.2007.08.005>
- Kivelson, M. G. (2004). Moon-magnetosphere interactions: A tutorial. *Advances in Space Research*, 33, 2061–2077. <https://doi.org/10.1016/j.asr.2003.08.042>
- Kotova, A. (2016). Energetic particle tracking techniques and its application to the magnetosphere of Saturn. (Theses). France: University of Toulouse, Université Toulouse III – Paul Sabatier. <https://tel.archives-ouvertes.fr/tel-01401253>
- Kotova, A., Roussos, E., Kollmann, P., Krupp, N., & Dandouras, I. (2019). Galactic cosmic rays access to the magnetosphere of Saturn. *Journal of Geophysical Research: Space Physics*, 124, 166–177. <https://doi.org/10.1029/2018JA025661>
- Kotova, A., Roussos, E., Krupp, N., & Dandouras, I. (2015). Modeling of the energetic ion observations in the vicinity of Rhea and Dione. *Icarus*, 258, 402–417. <https://doi.org/10.1016/j.icarus.2015.06.031>
- Krimigis, S. M., Mitchell, D. G., Hamilton, D. C., Livi, S., Dandouras, J., Jaskulek, S., et al. (2004). Magnetosphere Imaging Instrument (MIMI) on the Cassini Mission to Saturn/Titan. *Space Science Reviews*, 114, 233–329. <https://doi.org/10.1007/s11214-004-1410-8>
- Krupp, N., Roussos, E., Kriegel, H., Kollmann, P., Kivelson, M. G., Kotova, A., et al. (2013). Energetic particle measurements in the vicinity of Dione during the three Cassini encounters 2005–2011. *Icarus*, 226, 617–628. <https://doi.org/10.1016/j.icarus.2013.06.007>
- Liuzzo, L., Simon, S., & Regoli, L. (2019a). Energetic ion dynamics near Callisto. *Planetary Space Science*, 166, 23–53. <https://doi.org/10.1016/j.pss.2018.07.014>
- Liuzzo, L., Simon, S., & Regoli, L. (2019b). Energetic electron dynamics near Callisto. *Planetary and Space Science*, 179, 104726. <https://doi.org/10.1016/j.pss.2019.104726>
- Müller, J., Simon, S., Motschmann, U., Schüle, J., Glassmeier, K.-H., & Pringle, G. J. (2011). A.I.K.E.F.: Adaptive hybrid model for space plasma simulations. *Computer Physics Communications*, 182, 946–966. <https://doi.org/10.1016/j.cpc.2010.12.033>
- Paonessa, M., & Cheng, A. F. (1985). A theory of satellite sweeping. *Journal of Geophysical Research*, 90, 3428–3434. <https://doi.org/10.1029/JA090iA04p03428>
- Roussos, E., Andriopoulou, M., Krupp, N., Kotova, A., Paranasas, C., Krimigis, S. M., & Mitchell, D. G. (2013). Numerical simulation of energetic electron microsignature drifts at Saturn: Methods and applications. *Icarus*, 226, 1595–1611. <https://doi.org/10.1016/j.icarus.2013.08.023>

- Roussos, E., Kollmann, P., Krupp, N., Kotova, A., Regoli, L., Paranicas, C., et al. (2018). A radiation belt of energetic protons located between saturn and its rings. *Science*, 362, 6410. <https://doi.org/10.1126/science.aat1962>
- Roussos, E., Kollmann, P., Krupp, N., Paranicas, C., Dialynas, K., Jones, G. H., et al. (2019). Sources, sinks, and transport of energetic electrons near Saturn's main rings. *Geophysical Research Letters*, 46, 3590–3598. <https://doi.org/10.1029/2018GL078097>
- Roussos, E., Krupp, N., Armstrong, T. P., Paranicas, C., Mitchell, D. G., Krimigis, S. M., et al. (2008). Discovery of a transient radiation belt at Saturn. *Geophysical Research Letters*, 35, 22106. <https://doi.org/10.1029/2008GL035767>
- Roussos, E., Krupp, N., Paranicas, C., Carberry, J. F., Kollmann, P., Krimigis, S. M., & Mitchell, D. G. (2014). The variable extension of Saturn's electron radiation belts. *Planetary Space Science*, 104, 3–17. <https://doi.org/10.1016/j.pss.2014.03.021>
- Roussos, E., Krupp, N., Paranicas, C., Kollmann, P., Mitchell, D. G., Krimigis, S. M., & Palmaerts, B. (2018). Heliospheric conditions at Saturn during Cassini's ring-grazing and proximal orbits. *Geophysical Research Letters*, 45, 10,812–10,818. <https://doi.org/10.1029/2018GL078093>
- Saur, J., & Strobel, D. F. (2005). Atmospheres and plasma interactions at Saturn's largest inner icy satellites. *Applied Physical Journal*, 620, L115–L118. <https://doi.org/10.1086/428665>
- Sergis, N., Arridge, C. S., Krimigis, S. M., Mitchell, D. G., Rymer, A. M., Hamilton, D. C., et al. (2011). Dynamics and seasonal variations in Saturn's magnetospheric plasma sheet, as measured by Cassini. *Journal of Geophysical Research*, 116, A04203. <https://doi.org/10.1029/2010JA016180>
- Sergis, N., Krimigis, S. M., Mitchell, D. G., Hamilton, D. C., Krupp, N., Mauk, B. H., et al. (2009). Energetic particle pressure in Saturn's magnetosphere measured with the Magnetospheric Imaging Instrument on Cassini. *Journal of Geophysical Research*, 114, 2214. <https://doi.org/10.1029/2008JA013774>
- Simon, S., Roussos, E., & Paty, C. S. (2015). The interaction between Saturn's moons and their plasma environments. *Physics Reports*, 602, 1–65. <https://doi.org/10.1016/j.physrep.2015.09.005>
- Simon, S., Saur, J., Neubauer, F. M., Wennmacher, A., & Dougherty, M. K. (2011). Magnetic signatures of a tenuous atmosphere at Dione. *Geophysical Research Letters*, 38, 15102. <https://doi.org/10.1029/2011GL048454>
- Smith, E. J., & Tsurutani, B. T. (1983). Saturn's magnetosphere: Observations of ion cyclotron waves near the Dione I shell. *Journal of Geophysical Research*, 88(A10), 7831–7836. <https://doi.org/10.1029/JA088iA10p07831>
- Teolis, B. D., Jones, G. H., Miles, P. F., Tokar, R. L., Magee, B. A., Waite, J. H., et al. (2010). Cassini finds an oxygen-carbon dioxide atmosphere at Saturn's icy moon Rhea. *Science*, 330, 1813. <https://doi.org/10.1126/science.1198366>
- Teolis, B. D., & Waite, J. H. (2016). Dione and Rhea seasonal exospheres revealed by Cassini CAPS and INMS. *Icarus*, 272, 277–289. <https://doi.org/10.1016/j.icarus.2016.02.031>
- Thomsen, M. F., & van Allen, J. A. (1980). Motion of trapped electrons and protons in Saturn's inner magnetosphere. *Journal of Geophysical Research*, 85(A11), 5831–5834.
- Tokar, R. L., Johnson, R. E., Thomsen, M. F., Sittler, E. C., Coates, A. J., Wilson, R. J., et al. (2012). Detection of exospheric O<sub>2</sub><sup>+</sup> at Saturn's moon Dione. *Geophysical Research Letters*, 39, 3105. <https://doi.org/10.1029/2011GL050452>
- Tsintikidis, D., Kurth, W. S., Gurnett, D. A., & Barbosa, D. D. (1995). Study of dust in the vicinity of Dione using the Voyager 1 plasma wave instrument. *Journal of Geophysical Research*, 100, 1811–1822. <https://doi.org/10.1029/94JA02357>
- Wilson, R. J., Bagenal, F., & Persoon, A. M. (2017). Survey of thermal plasma ions in Saturn's magnetosphere utilizing a forward model. *Journal of Geophysical Research: Space Physics*, 122, 7256–7278. <https://doi.org/10.1002/2017JA024117>